ACS APPLIED MATERIALS & INTERFACES

Research Article

www.acsami.org

High-Efficiency Aqueous-Solution-Processed Hybrid Solar Cells Based on P3HT Dots and CdTe Nanocrystals

Shiyu Yao,[†,⊥] Zhaolai Chen,[†,⊥] Fenghong Li,[†] Bin Xu,[†] Jiaxing Song,[†] Lulin Yan,[†] Gan Jin,[‡] Shanpeng Wen,[§] Chen Wang,[§] Bai Yang,[†] and Wenjing Tian*[,†]

[†]State Key Laboratory of Supramolecular Structure and Materials, Jilin University, Changchun 130012, P. R. China

[‡]College of Chemistry, Northeast Normal University, Changchun 130024, P. R. China

[§]State Key Laboratory on Integrated Optoelectronics, Jilin University, Changchun 130012, P. R. China

Supporting Information

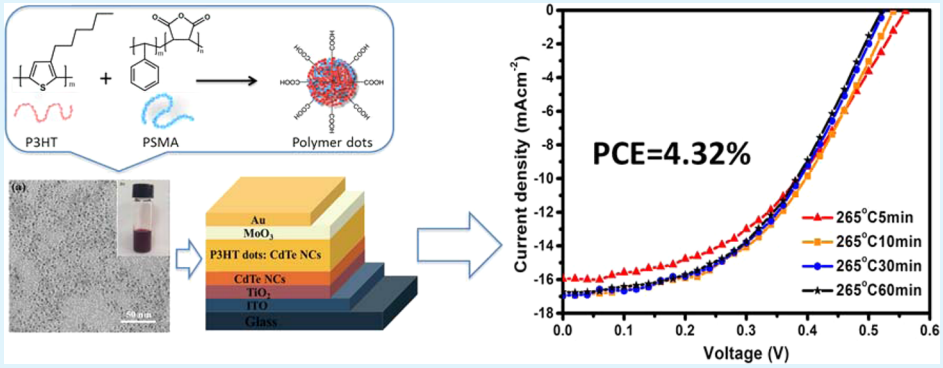

ABSTRACT: Without using any environmentally hazardous organic solution, we fabricated hybrid solar cells (HSCs) based on the aqueous-solution-processed poly(3-hexylthiophene) (P3HT) dots and CdTe nanocrystals (NCs). As a novel aqueous donor material, the P3HT dots are prepared through a reprecipitation method and present an average diameter of 2.09 nm. When the P3HT dots are mixed with the aqueous CdTe NCs, the dependence of the device performance on the donor−acceptor ratio shows that the optimized ratio is 1:24. Specifically, the dependence of the device performance on the active-layer thermal annealing conditions is investigated. As a result, the optimized annealing temperature is 265 °C, and the incorporation of P3HT dots as donor materials successfully reduced the annealing time from 1 h to 10 min. In addition, the transmission electron microscopy and atomic force microscopy measurements demonstrate that the size of the CdTe NCs increased as the annealing time increased, and the annealing process facilitates the formation of a smoother interpenetrating network in the active layer. Therefore, charge separation and transport in the P3HT dots:CdTe NCs layer are more efficient. Eventually, the P3HT dots:CdTe NCs solar cells achieved 4.32% power conversion efficiency. The polymer dots and CdTe NCs based aqueous-solution-processed HSCs provide an effective way to avoid a long-time thermal annealing process of the P3HT dots:CdTe NCs layer and largely broaden the donor materials for aqueous HSCs.

KEYWORDS: *polymer dots, aqueous-solution-processed, hybrid solar cells, inorganic nanocrystals*

1. INTRODUCTION

Combining the high-electron-mobility, tunable absorption of inorganic nanocrystals (NCs) with the solution processability of polymers, the hybrid solar cells (HSCs) become a promising candidate of high-efficiency, low-cost, and flexible photovoltaic devices.[1−6] Since the pioneering work of Alivisatos and co-workers,[1] significant improvement of the HSC performance has been made and a power conversion efficiency (PCE) of 5.5% has been achieved.[7] However, the most successful and widely used solvents in the fabrication process of HSCs are chlorinated and aromatic solvents, which are flammable and detrimental to human health and the environment and use a high amount of electrical energy during production.[8−10] Compared with these organic solvents, water is green and biocompatible. Therefore, aqueous processing without using environmentally hazardous organic solvents was introduced in the fabrication of HSCs by making efficient photovoltaic devices through environmentally friendly and safe procedures. McLeskey et al. first introduced aqueous processing in HSCs based on poly[2-(3-thienyl)-ethoxy-4-butylsulfonate] and TiO_2.[11−13] Manca et al. reported HSCs based on a water-soluble derivative of polythiophene and TiO_2 nanoparticles or nanorods, and a PCE of 0.7% was achieved.[14−17]

Received: December 20, 2014
Accepted: March 17, 2015
Published: March 17, 2015

DOI: 10.1021/am508985q
ACS Appl. Mater. Interfaces 2015, 7, 7146−7152

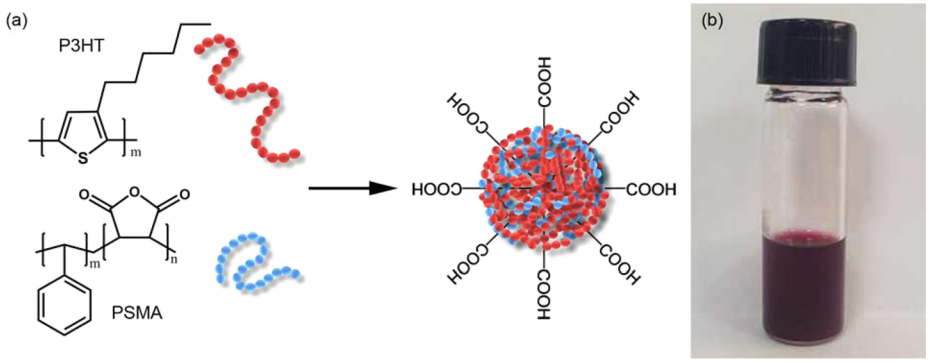

Figure 1. (a) Formation of P3HT dots. (b) Picture of a P3HT dots solution.

Nevertheless, the performance of the water-soluble conjugated polymer and TiO_2 based HSCs was relatively poor because of the weak absorption of TiO_2. To achieve higher PCEs of aqueous HSCs, Yang and co-workers introduced CdTe NCs as the acceptor to increase the device absorption and a polymer precursor instead of a water-soluble polymer as the donor.[18] They improved the performance of the aqueous CdTe NCs/polymer precursors based HSCs from 2.14% to 4.76% by using different polymer precursors and interfacial modification materials, changing the donor−acceptor ratio, and optimizing the thermal annealing condition of the active layer.[19−27] However, the polymer precursors for aqueous HSCs only involved phenylene, thiophene, and naphthalene derivatives, which are not well developed. Moreover, the active layer based on CdTe NCs and polymer precursors required a long-time annealing process of at least 1 h to promote polymerization of the polymer precursor and growth of CdTe NCs, which is complicated and wastes energy during the fabrication process.

As we know, a large number of conjugated polymers with good photovoltaic properties have been developed for polymer solar cells in the last 2 decades.[28−32] The application of these conjugated polymers to aqueous HSCs will largely develop the donor materials for aqueous HSCs. Also, polymer nanoparticles or polymer dots (Pdots; particle size < 20−30 nm)[33] exactly provide a way to transfer the conjugated polymer from organic solvents to an aqueous phase. For example, Krebs et al. incorporated the aqueous polymer/1-(methoxycarbonylpropyl)-1-phenyl-[6.0]C61 (PCBM) nanoparticles into the aqueous-solution-processed polymer solar cells and achieved a PCE of 0.55% for a large-scale roll-to-roll device.[8] Dastoor et al. have reported an approach for producing optimized organic solar cells from polyfluorene nanoparticles.[34] Recently, Belcher et al. reported organic photovoltaics based on a surfactant-free poly(3-hexylthiophene) (P3HT):PCBM nanoparticulate with a PCE of 1.09%.[35]

Herein, the aqueous polymer dots, which were prepared from the conjugated polymer P3HT, were first introduced as the donor materials for aqueous HSCs. Also, aqueous HSCs with the structure of indium−tin oxide (ITO)/TiO_2/CdTe NCs/P3HT dots:CdTe NCs/MoO_3/Au were fabricated by using aqueous P3HT dots (2.09 nm) and aqueous CdTe NCs (3.32 nm). The investigation of the dependence of the performance on the donor−acceptor weight ratio indicated the optimized P3HT dots: CdTe NCs ratio is 1:24 and the device showed a 4.12% PCE. We especially investigated the influence of the thermal annealing temperature and time of the P3HT dots:CdTe NCs layer on the device efficiency. Remarkably, we successfully reduced the annealing time of the P3HT dots:CdTe NCs layer from 1 h to 10 min by the introduction of the P3HT dots. The best device performance with 16.95 mA cm^{-2} short-circuit current (J_{sc}), 0.54 V open-circuit voltage (V_{oc}), 47.2% fill factor (FF), and 4.32% PCE was achieved when thermally annealed at 265 °C for 10 min. The transmission electron microscopy (TEM) and atomic force microscopy (AFM) measurements showed that a 265 °C and 10 min annealing process facilitated the formation of a smoother interpenetrating network in the active layer, which resulted in more efficient charge separation and transport in the P3HT dots:CdTe NCs layer and the interface between the P3HT dots:CdTe NCs layer and MoO_3. The polymer dots and CdTe NCs based aqueous-solution-processed HSCs provided an effective way to avoid a long-time thermal annealing process of the P3HT dots:CdTe NCs layer and largely broaden the donor materials for aqueous HSCs.

2. EXPERIMENTAL SECTION

2.1. Materials. Tetrahydrothiophene (99%), poly(styrene-*co*-maleic anhydride) (PSMA), tellurium powder (200 mesh, 99.8%), and α,α'-dichloro-*p*-xylene (98%) were all obtained from Aldrich. Cadmium chloride hemipentahydrate (99%), chloroauric acid (analytical reagant, AR), and sodium borohydride (99%) were commercially obtained from Sinopharm Chemical Reagent Co. Ltd. Poly(3-hexylthiophene) (P3HT) was from Rieke Metals. Molybdenum oxide (>99%) and 2-mercaptoethylamine (MA; 98%) were purchased from Acros. Sodium citrate, isopropyl alcohol, methanol, acetone, and *n*-hexane were AR grade. All materials were used as received.

2.2. Preparation of P3HT Dots. Water-soluble P3HT dots were prepared through a reprecipitation method. PSMA (1 mg mL^{-1}) and P3HT (5 mg mL^{-1}) were dissolved and mixed in tetrahydrofuran (THF) and stirred for 4 h until homogeneous. A total of 10 mL of deionized water was sonicated in a bath sonicator. At the same time, 5 mL of a P3HT and PSMA mixed solution was injected into deionized water and sonicated for 30 min. After that, a stream of N_2 gas went through the solution to remove THF and concentrate the solution on a 90 °C hot plate. Finally, upon filtration through a 0.2 μm filter, the P3HT dots solution was produced.

2.3. Synthesis of CdTe NCs. Synthesis of CdTe NCs was performed following the previous report.[18] MA was added into a 12.5 mM $CdCl_2$ aqueous solution, and the pH was adjusted to 5.70−5.74. A total of 0.28 mL of a NaHTe(2/3M) solution was added into a N_2-saturated MA and $CdCl_2$ mixed solution. The molar ratio of Cd/Te/MA was 1:0.2:2.4. Growth of CdTe NCs was obtained by refluxing the mixed solution at 100 °C for 30 min. Then the CdTe NCs solution was concentrated to 8 mL and cooled to room temperature. After that, the CdTe NCs solution was centrifuged for 5 min at 6000 rpm in the presence of isopropyl alcohol. Using a vacuum oven, the CdTe NCs were dried at room temperature. Finally the CdTe NCs were dissolved

DOI: 10.1021/am508985q
ACS Appl. Mater. Interfaces 2015, 7, 7146−7152

in 1 mL of deionized water and reached a concentration of 72 mg mL^{-1}.

2.4. Device Fabrication. The ITO substrate was cleaned by ethanol, acetone, isopropyl alcohol, and N_2 flow. Next, the ITO substrate was treated by O_2 plasma for 10 min. The TiO_2 precursor (tetrabutyltitanate) was spin-coated onto the ITO with a speed of 2000 rpm and then annealed at 350 °C for 15 min to produce the anatase TiO_2. The CdTe NCs solution was spin-coated onto the TiO_2 layer at 700 rpm for 40 s in the air, with an annealing process in N_2 at 265 °C for 2 min. After that, the mixed P3HT dots and CdTe NCs solution with different ratios was spin-coated at 700 rpm for 40 s with a repeated annealing process at 265 °C for 2 min in N_2. Then another P3HT dots:CdTe NCs layer was fabricated and annealed at 265 °C in the glovebox for different times. Finally, MoO_3 (5 nm) and Au (80 nm) were deposited on the P3HT dots:CdTe NCs layer through vacuum evaporation at a pressure below 10^{-5} Torr, with a 5 mm^2 active area.

2.5. Characterization. UV−vis absorption spectra of the P3HT dots and CdTe NCs films were measured by a Shimadzu 3600 UV−vis−near-IR spectrophotometer. A Hitachi H-800 electron microscope was used to conduct TEM with a CCD camera at an acceleration voltage of 200 kV. The SII Nanonavi probe station (300hv) was used to perform the AFM measurements. An integrated ultrahigh-vacuum system equipped with a multitechnique surface analysis system (VG Scienta R3000) for ultraviolet photoelectron spectroscopy (UPS) was used to obtain the energy band values. Under AM1.5G 100 mW cm^{-2} illumination, a computer-controlled Keithley 2400 sourcemeter system was used to measure the current density versus voltage (J−V) characteristics. A Crowntech QTest Station 1000AD was used to measure the external quantum efficiency (EQE).

3. RESULTS AND DISCUSSION

3.1. Preparation and Basic Properties of P3HT Dots and CdTe NCs. P3HT dots were prepared by using a reprecipitation method. Compared with the typical miniemulsion approach, the reprecipitation method exhibited higher yield and reliably generated Pdots with a size of 5−30 nm rather than polymer nanoparticles of 40−500 nm.[33] In the procedure, a solution of P3HT and a commercial copolymer, PSMA, dissolved in THF was added to water and sonicated. During the process of Pdots formation, the P3HT chains and the hydrophobic polystyrene part of PSMA were likely intertwined with each other and anchored inside the body of Pdots. At the same time, maleic anhydride units hydrolyzed in water resulted in Pdots surface-localized carboxyl groups (Figure 1a).[38] After formation of Pdots, the organic solvent was removed under a N_2 flow and heating process. With the carboxyl groups covering the outside, Pdots were dispersed in water and exhibited a clear aqueous solution that was stable for several months (Figure 1b). The TEM images of the P3HT dots solution were analyzed to determine their morphologies and size distributions. As we can see from the TEM images (Figure 2a), the P3HT dots are spherical, with an average diameter of approximately 2.09 nm. The statistical size distribution of the P3HT dots is shown in Figure 2b. Because 2.09 nm is shorter than the exciton diffusion length of the conjugated polymer, it is reasonable to believe that the as-prepared P3HT dots will facilitate exciton dissociation and charge separation at the interface between P3HT dots and CdTe NCs. Thermal gravimetric analysis (TGA) of P3HT and PSMA in Figure S1 in the Supporting Information (SI) shows that P3HT and PSMA have excellent stabilities with decomposition temperatures of 463 and 316 °C, respectively. The absorption spectra of the as-prepared and annealed P3HT dots films are shown in Figure S2a in the SI. The absorption of the P3HT dots film ranged from 300 to 750 nm as the regular P3HT film.

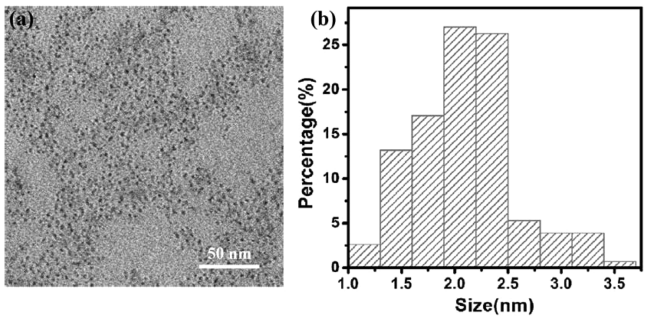

Figure 2. (a) TEM image of P3HT dots. (b) P3HT dots size distribution based on 152 dots.

CdTe NCs were synthesized according to the previous report.[27] TEM images of CdTe NCs before annealing are shown in Figure S3 in the SI. It is observed that the as-prepared CdTe NCs exhibit an average diameter of approximately 3.32 nm. Figure S2b in the SI shows the absorption spectra of the as-prepared CdTe NCs film and the CdTe NCs film annealed at 265 °C for 10 min. After annealing, the CdTe NCs grew bigger and the absorption peak of the CdTe film red shifted from 511 to 824 nm.

The UPS spectrum of CdTe is shown in Figure S4 in the SI, and the valence (VB) and conduction (CB) bands (−6.19 and −4.69 eV, respectively) of fully grown CdTe NCs are obtained from analysis of the UPS measurements, as shown in Figure 3a, together with the lowest unoccupied molecular orbital

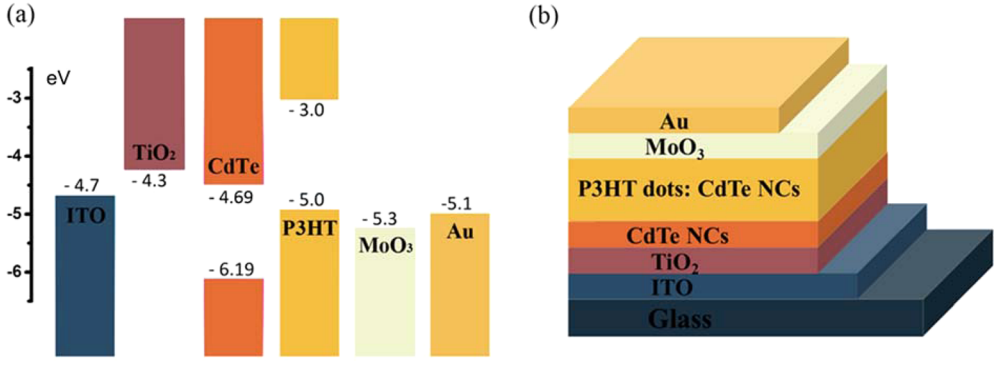

Figure 3. (a) Energy-level diagram of the P3HT dots:CdTe NCs solar cell. (b) P3HT dots:CdTe NCs solar cell device structure.

DOI: 10.1021/am508985q
ACS Appl. Mater. Interfaces 2015, 7, 7146−7152

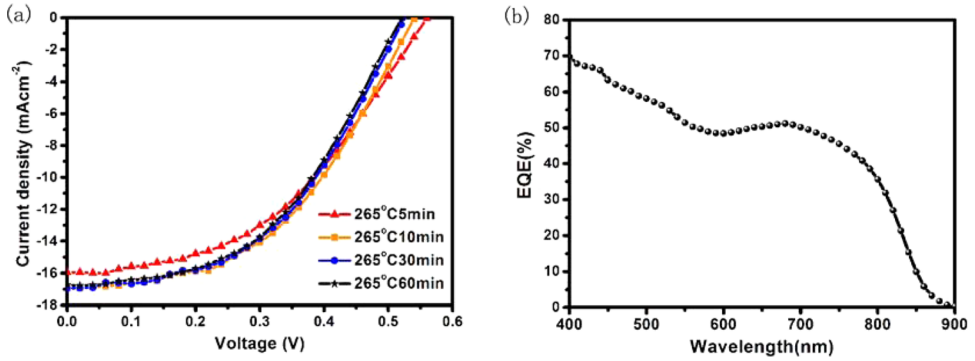

Figure 4. (a) $J-V$ curves of the P3HT dots:CdTe NCs solar cell devices annealed at 265 °C for 5, 10, 30, and 60 min. (b) EQE curve of the P3HT dots:CdTe NCs solar cell device annealed at 265 °C for 10 min.

Table 1. Device Performance with Different Annealing Times of 5, 10, 30, and 60 min

annealing time [min]	J_{sc} [mA cm^{-2}]	V_{oc} [V]	FF [%]	PCE [%]	rms roughness [nm]
5	15.95	0.56	45.1	4.03	4.358
10	16.95	0.54	47.2	4.32	4.288
30	16.94	0.52	48.2	4.25	5.527
60	16.73	0.52	47.6	4.14	5.813

(LUMO) and highest occupied molecular orbital (HOMO) of P3HT as well as the relative energy levels of TiO_2 and MoO_3. The VB value of CdTe (−6.19 eV) is calculated from the UPS measurements. The VB value was calculated by subtracting the onset of the low-binding-energy photoemission from the onset of the secondary electron energy cutoff and then subtracting the excitation photoenergy (21.2 eV).

3.2. Aqueous-Solution-Processed HSCs Based on P3HT Dots and CdTe NCs. The device structure of the HSC is ITO/TiO_2/CdTe NCs/P3HT dots:CdTe NCs/MoO_3/Au (Figure 3b). MoO_3 is chosen as the hole-transport material, and TiO_2 is selected as the electron-transport material. In order to enhance the light absorption and electron selectivity, a single CdTe NCs layer was introduced between the P3HT dots:CdTe NCs and TiO_2 layers.[26]

The device performances of the solar cells usually greatly depend on the ratio of the donor and acceptor. When P3HT dots was mixed with CdTe NCs, the ratio dependence of P3HT dots:CdTe NCs based solar cells was investigated, and the results are presented in Figure S5 and Table S1 in the SI. When the P3HT dots:CdTe NCs weight ratio was 1:36, the device exhibited J_{sc} of 13.03 mA cm^{-2}, V_{oc} of 0.52 V, FF of 46.6%, and PCE of 3.16%. In this case, the content of P3HT dots is too low and charge transport is poor, which causes the relatively low short-circuit current. When the content of P3HT dots was increased and the ratio was 1:18, the electrostatic force interaction between the negative charges on the surface of CdTe NCs and positive charges on the surface of P3HT dots increased and caused the appearance of precipitation in the blend solution, which formed an inhomogeneous active layer. The precipitate in the P3HT dots:CdTe NCs layer hindered charge transport and decreased J_{sc} to 12.61 mA cm^{-2}, FF to 35.1%, and PCE to 2.3%. An optimized PCE of 4.12% was achieved when the ratio became 1:24, and J_{sc} increased to 16.57 mA cm^{-2} with FF of 47.8% and V_{oc} of 0.52 V.

Because the thermal annealing process plays a direct and important role in influencing the quality and property of the P3HT dots:CdTe NCs layer, the effect of the annealing temperature and time of the P3HT dots:CdTe NCs layer on the device performance of P3HT dots:CdTe NCs based aqueous HSCs was investigated. Compared with the previously reported polymer precursor/CdTe NCs system, P3HT dots does not require an annealing process to confirm polymerization of a polymer with high molecular weight. In terms of CdTe NCs, the annealing process was necessary to promote removal of the surface ligands on CdTe NCs and growth of CdTe NCs.[18]

The influence of the annealing temperature on the device performance was investigated with the temperature varied from 160 to 320 °C, and the $J-V$ characteristics are shown in Figure S6 and Table S2 in the SI. When the temperature was 160 °C, J_{sc} and FF were only 0.66 mA cm^{-2} and 24.1%, which lead to a poor PCE of 0.08%. The results indicated that the interfacial ligands on CdTe NCs were not removed when the active layer was annealed at 160 °C, which hindered charge dissociation and transport in the active layer. When the temperature was increased to 210 °C, J_{sc} of 10.77 mA cm^{-2} and PCE of 2.15% were obtained, which indicated that ligand deprival on the

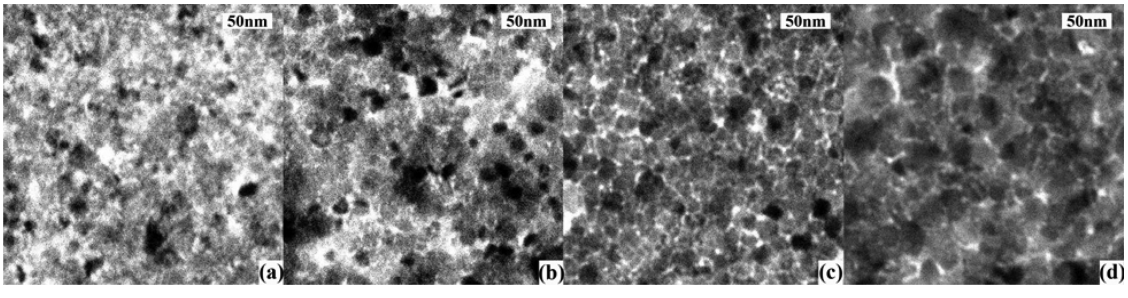

Figure 5. TEM images of the P3HT dots:CdTe NCs blended films annealed at 265 °C for (a) 5, (b) 10, (c) 30, and (d) 60 min.

DOI: 10.1021/am508985q
ACS Appl. Mater. Interfaces 2015, 7, 7146−7152

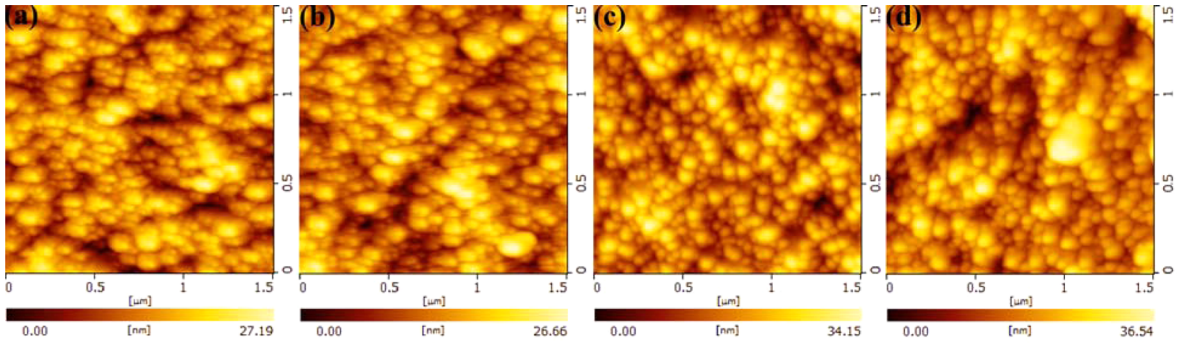

Figure 6. Topographic AFM images (1.5 μm × 1.5 μm) of the P3HT dots:CdTe NCs blended films annealed at 265 °C for (a) 5, (b) 10, (c) 30, and (d) 60 min.

CdTe NCs occurred. When the annealing temperature was further increased to 265 °C, the performance with J_{sc} of 16.05%, V_{oc} of 0.54, FF of 42.7%, and PCE of 3.7% was achieved. The high temperature (265 °C) promoted elimination of the ligands on CdTe NCs and further facilitated charge dissociation and transport in the active layer. However, the higher temperature (320 °C) decreased J_{sc}, V_{oc}, and PCE to 13.4 mA cm^{-2}, 0.46 V, and 2.94%, maybe because of decomposition of PSMA. The results suggested that the optimized annealing temperature of the active layer was 265 °C.

To investigate the dependence of the performance on the annealing time, the active layers were annealed for 5, 10, 30, and 60 min at 265 °C. The photovoltaic performances of HSCs annealed for different times are shown in Figure 4a. When the active layer was annealed for only 5 min, PCE of 4.03% had already been reached with V_{oc} of 0.56 V, J_{sc} of 15.95 mA cm^{-2}, and FF of 45.1%. When the annealing time was increased from 5 to 10 min, J_{sc} increased from 15.95 to 16.95 mA cm^{-2}, and FF was improved to 47.2%, while V_{oc} decreased to 0.54 V and PCE of 4.32% was achieved. Upon annealing for 30 min, there are only slight changes in J_{sc} (from 16.95 to 16.94 mA cm^{-2}), FF (from 47.2 to 48.2%), V_{oc} (from 0.54 to 0.52 V), and PCE (from 4.32 to 4.25%). Upon 60 min of annealing, the device gave J_{sc} of 16.73 mA cm^{-2}, V_{oc} of 0.52 V, FF of 47.6%, and PCE of 4.14%. The optimized device was obtained by annealing the P3HT dots:CdTe NCs layer at 265 °C for 10 min. The performances of devices with different annealing times are summarized in Table 1, which indicates that the P3HT dots:CdTe NCs based HSCs only need 10 min of annealing at 265 °C.

To understand the changes in the device performance with different thermal annealing times of the active layer, TEM and AFM of the active layer were measured to observe the differences in the morphology and surface topography. Upon annealing for only 5 min, the TEM image (Figure 5a) shows that CdTe NCs grew from 3.32 to 7.83 nm and the sizes of the P3HT dots domains were in the range of 9−19 nm. The AFM image in Figure 6a shows that the active layer exhibits a relatively rough surface and the root-mean-square (rms) roughness is 4.358 nm. When the annealing time lasted for 10 min, as shown in Figure 5b, the CdTe NCs grew from 7.83 to 11.26 nm with a more uniform distribution and became interconnected with each other, which formed a continuous electron-transport pathway. The sizes of P3HT dots domains were in the range of 6−15 nm, and the P3HT dots formed an effective hole-transport channel. Therefore, 10 min thermal annealing promoted formation of an interpenetrating network in the P3HT dots:CdTe NCs layer, which enhanced charge separation and transport, avoided the occurrence of pinholes, and increased J_{sc} from 15.95 to 16.95 mA cm^{-2}. Meanwhile, a homogeneous active layer formed and exhibited a rms roughness of 4.288 nm. Thus, the active layer presented the smoothest morphology, which is beneficial to a better interface contact between the P3HT dots:CdTe NCs and MoO_3 layers, and improved FF from 45.1% to 47.2%. When the annealing time was increased to 30 and 60 min, the sizes of the CdTe NCs grew to 15.41 and 20.13 nm, as shown in Figure 5c,d, and the rms roughness largely increased from 4.288 to 5.527 and 5.813 nm. Meanwhile, large-sized CdTe nanoclusters appeared in the larger-scale-viewed 5 μm × 5 μm AFM topographic images (Figure S7 in the SI) of the 30 and 60 min annealed active layers. Even though CdTe has formed a continuous electron-transport phase, the large CdTe clusters resulted in an inhomogeneous film with large-scale phase separation, which adversely influenced charge separation and transport in the P3HT dots:CdTe NCs layer as well as charge transport between the P3HT dots:CdTe NCs layer and MoO_3. Therefore, J_{sc} and PCE decreased to 16.94 mA cm^{-2} and 4.25% and 16.73 mA cm^{-2} and 4.14%. It is noted that V_{oc} decreased from 0.56 to 0.52 V as the annealing time increased, which may be due to the higher crystallinity of the P3HT film, leading to an upward shift of the P3HT HOMO level.[36,37] The optimized thermal annealing condition is 265 °C for 10 min, with the highest PCE of 4.23%, V_{oc} of 0.54 V, J_{sc} of 16.95 mA cm^{-2}, and FF of 47.2%, with a 4.288 nm rms roughness for the P3HT dots:CdTe NCs layer.

To check the reproducibility of the performance, a histogram of the average PCEs for the devices contributing to our work is presented. As shown in Figure S9 in the SI, around 70% of the devices exhibited an overall efficiency exceeding 3.5% under 1 sun condition. Of those, 30% have PCEs higher than 4%.

The EQE of the device annealed at 265 °C for 10 min is plotted in Figure 4b. It is observed that the device presents a wide spectral response from 400 to 900 nm and reaches its maximum value of 70% at 400 nm.

4. CONCLUSION

In conclusion, we reported the incorporation of the aqueous polymer dots as the donor and aqueous CdTe NCs as the acceptor in aqueous HSCs. By using a reprecipitation method, P3HT dots exhibited a 2.09 nm average diameter and were prepared from the classic conjugated polymer P3HT. The influence of the P3HT dots:CdTe NCs weight ratio on the device performance indicated that the optimized P3HT

DOI: 10.1021/am508985q
ACS Appl. Mater. Interfaces 2015, 7, 7146−7152

dots:CdTe NCs ratio was 1:24, and PCE of 4.12% was achieved. The dependence of the device performance on the thermal annealing condition demonstrated that the optimized annealing temperature of the active layer was 265 °C. Also, we notably reduced the thermal annealing time from 1 h to 10 min and achieved J_{sc} of 16.95 mA cm^{-2}, V_{oc} of 0.54 V, FF of 47.2%, and PCE of 4.32% because of formation of the interpenetrating network in the active layer and the smooth surface morphology of the P3HT dots:CdTe NCs layer. The aqueous-solution-processed HSCs based on polymer dots and CdTe NCs provided a new, versatile, and promising approach for further research to lead to high-performance aqueous HSCs.

■ ASSOCIATED CONTENT

Supporting Information

TGA curves of PSMA and P3HT, UV−vis absorption spectra of the P3HT dots and CdTe NCs films, TEM image of CdTe NCs before annealing, UPS spectrum of the CdTe cutoff and Fermi-edge regions, photovoltaic and device performances of devices with different P3HT dots to CdTe NCs ratios and different annealing temperatures, topographic AFM images of the P3HT dots:CdTe NCs blended films annealed at different times, and a histogram of PCEs. This material is available free of charge via the Internet at http://pubs.acs.org.

■ AUTHOR INFORMATION

Corresponding Author

*E-mail: wjtian@jlu.edu.cn.

Author Contributions

⊥These authors contributed equally to this work.

Notes

The authors declare no competing financial interest.

■ ACKNOWLEDGMENTS

This work was supported by the Natural Science Foundation of China (Grant 21221063), 973 Program (Grant 2014CB643506), Program for Chang Jiang Scholars and Innovative Research Team in University (Grant IRT101713018), and the Graduate Innovation Fund of Jilin University (Grant 450060503118).

■ REFERENCES

(1) Huynh, W. U.; Dittmer, J. J.; Alivisatos, A. P. Hybrid Nanorod-Polymer Solar Cells. *Science* **2002**, *29*, 2425−2427.

(2) Borchert, H. Elementary Processes and Limiting Factors in Hybrid Polymer/Nanoparticle Solar Cells. *Energy Environ. Sci.* **2010**, *3*, 1682−1694.

(3) Dowland, S.; Lutz, T.; Ward, A.; King, S. P.; Sudlow, A.; Hill, M. S.; Molloy, K. C.; Haque, S. A. Direct Growth of Metal Sulfide Nanoparticle Networks in Solid-State Polymer Films for Hybrid Inorganic−Organic Solar Cells. *Adv. Mater.* **2011**, *23*, 2739−2744.

(4) Seo, J.; Cho, M. J.; Lee, D.; Cartwright, A. N.; Prasad, P. N. Efficient Heterojunction Photovoltaic Cell Utilizing Nanocomposites of Lead Sulfide Nanocrystals and a Low-Bandgap Polymer. *Adv. Mater.* **2011**, *23*, 3984−3988.

(5) Debnath, R.; Bakr, O.; Sargent, E. H. Solution-Processed Colloidal Quantum Dot Photovoltaics: A Perspective. *Energy Environ. Sci.* **2011**, *4*, 4870−4881.

(6) Yip, H.-L.; Jen, A. K.-Y. Recent Advances in Solution-Processed Interfacial Materials for Efficient and Stable Polymer Solar Cells. *Energy Environ. Sci.* **2012**, *5*, 5994−6011.

(7) Liu, Z.; Yuan, J.; Wei, H.; Huang, X.; Han, L.; Wang, W.; Wang, H.; Ma, W. High-Efficiency Hybrid Solar Cells Based on Polymer/PbS_xSe_{1-x} Nanocrystals Benefiting from Vertical Phase Segregation. *Adv. Mater.* **2013**, *25*, 5772−5778.

(8) Andersen, T. R.; Larsen-Olsen, T. T.; Andreasen, B.; Böttiger, A. P. L.; Carlé, J. E.; Helgesen, M.; Bundgaard, E.; Norrman, K.; Andreasen, J. W.; Jørgensen, M.; Krebs, F. C. Aqueous Processing of Low-Band-Gap Polymer Solar Cells Using Roll-to-Roll Methods. *ACS Nano* **2011**, *5*, 4188−4196.

(9) Søndergaard, R.; Helgesen, M.; Jørgensen, M.; Krebs, F. C. Fabrication of Polymer Solar Cells Using Aqueous Processing for All Layers Including the Metal Back Electrode. *Adv.Energy Mater.* **2011**, *1*, 68−71.

(10) Chen, Y.; Zhang, S.; Wu, Y.; Hou, J. Molecular Design and Morphology Control Towards Efficient Polymer Solar Cells Processed using Non-aromatic and Non-chlorinated Solvents. *Adv. Mater.* **2014**, *26*, 2744−2749.

(11) Qiao, Q.; McLeskey, J. T. Water-Soluble Polythiophene/Nanocrystalline TiO_2 Solar Cells. *Appl. Phys. Lett.* **2005**, *86*, 153501−3.

(12) Qiao, Q.; Su, L.; Beck, J.; McLeskey, J. T. Characteristics of Water-soluble Polythiophene: TiO_2 Composite and its Application in Photovoltaics. *J. Appl. Phys.* **2005**, *98*, 094906−7.

(13) Qiao, Q.; Xie, Y.; McLeskey, J. T. Organic/Inorganic Polymer Solar Cells Using a Buffer Layer from All-Water-Solution Processing. *J. Phys. Chem. C* **2008**, *112*, 9912−9916.

(14) Baeten, L.; Conings, B.; D'Haen, J.; Hardy, A.; Manca, J. V.; Van Bael, M. K. Fully Water-Processable Metal Oxide Nanorods/Polymer Hybrid Solar Cells. *Sol. Energy Mater. Sol. Cells* **2012**, *107*, 230−235.

(15) Haeldermans, I.; Truijen, I.; Vandewal, K.; Moons, W.; Van Bael, M. K.; D'Haen, J.; Manca, J. V.; Mullens, J. Water Based Preparation Method for 'Green' Solid-state Polythiophene Solar Cells. *Thin Solid Films* **2008**, *516*, 7245−7250.

(16) Thalluri, G. K. V. V.; Bolsee, J.-C.; Gadisa, A.; Parchine, M.; Boonen, T.; D'Haen, J.; Boyukbayram, A. E.; Vandenbergh, J.; Cleij, T. J.; Lutsen, L.; Vanderzande, D.; Manca, J. Opto-electrical and Morphological Characterization of Water Soluble Conjugated Polymers for Eco-friendly Hybrid Solar Cells. *Sol. Energy Mater. Sol. Cells* **2011**, *95*, 3262−3268.

(17) Thalluri, G. K. V. V.; Bolsee, J.-C.; Madapati, S.; Vanmaekelbergh, D.; Manca, J. Study of Optical and Electrical Properties of Water-soluble Conjugated Poly(3-hexylthiophene) on Different Grain-sized Mesoporous TiO_2 Layers. *Thin Solid Films* **2014**, *556*, 285−290.

(18) Yu, W.; Zhang, H.; Fan, Z.; Zhang, J.; Wei, H.; Zhou, D.; Xu, B.; Li, F.; Tian, W.; Yang, B. Efficient Polymer/nanocrystal Hybrid Solar Cells Fabricated from Aqueous Materials. *Energy Environ. Sci.* **2011**, *4*, 2831−2834.

(19) Jin, G.; Wei, H.; Na, T.; Sun, H.; Zhang, H.; Yang, B. High-Efficiency Aqueous-Processed Hybrid Solar Cells with an Enormous Herschel Infrared Contribution. *ACS Appl. Mater. Interfaces* **2014**, *6*, 8606−8612.

(20) Fan, Z.; Zhang, H.; Yu, W.; Xing, Z.; Wei, H.; Dong, Q.; Tian, W.; Yang, B. Aqueous-Solution-Processed Hybrid Solar Cells from Poly(1,4-naphthalenevinylene) and CdTe Nanocrystals. *ACS Appl. Mater. Interfaces* **2011**, *3*, 2919−2923.

(21) Yu, W.; Zhang, H.; Tian, H.; Wei, H.; Liu, W.; Zhu, J.; Zhang, J.; Yang, B. Correlation between Annealing-Induced Growth of Nanocrystals and the Performance of Polymer: Nanocrystals Hybrid Solar Cells. *J. Phys. Chem. C* **2012**, *116*, 1322−1328.

(22) Chen, Z.; Zhang, H.; Xing, Z.; Hou, J.; Li, J.; Wei, H.; Tian, W.; Yang, B. Aqueous-Solution-Processed Hybrid Solar Cells with Good Thermal and Morphological Stability. *Sol. Energy Mater. Sol. Cells* **2013**, *109*, 254−261.

(23) Chen, Z.; Zhang, H.; Zeng, Q.; Wang, Y.; Xu, D.; Wang, L.; Wang, H.; Yang, B. In Situ Construction of Nanoscale CdTe−CdS Bulk Heterojunctions for Inorganic Nanocrystal Solar Cells. *Adv. Energy Mater.* **2014**, *4*, 1400235.

(24) Du, X.; Chen, Z.; Li, Z.; Hao, H.; Zeng, Q.; Dong, C.; Yang, B. Dip-Coated Gold Nanoparticle Electrodes for Aqueous-Solution-

DOI: 10.1021/am508985q
ACS Appl. Mater. Interfaces 2015, 7, 7146−7152

Processed Large-Area Solar Cells. *Adv. Energy Mater.* **2014**, *4*, 1400135.
(25) Wei, H.; Zhang, H.; Jin, G.; Na, T.; Zhang, G.; Zhang, X.; Wang, Y.; Sun, H.; Tian, W.; Yang, B. Coordinatable and High Charge-Carrier-Mobility Water-Soluble Conjugated Copolymers for Effective Aqueous-Processed Polymer−Nanocrystal Hybrid Solar Cells and OFET Applications. *Adv. Funct. Mater.* **2014**, *26*, 4035−4042.
(26) Chen, Z.; Zhang, H.; Du, X.; Cheng, X.; Chen, X.; Jiang, Y.; Yang, B. From Planar-Heterojunction to n−i Structure: an Efficient Strategy to Improve Short-circuit Current and Power Conversion Efficiency of Aqueous-Solution-Processed Hybrid Solar Cells. *Energy Environ. Sci.* **2013**, *6*, 1597−1603.
(27) Chen, Z.; Zhang, H.; Yu, W.; Li, Z.; Hou, J.; Wei, H.; Yang, B. Inverted Hybrid Solar Cells from Aqueous Materials with a PCE of 3.61%. *Adv. Energy Mater.* **2013**, *3*, 433−437.
(28) Blouin, N.; Michaud, A.; Gendron, D.; Wakim, S.; Blair, E.; Neagu-Plesu, R.; Belletete, M.; Durocher, G.; Tao, Y.; Leclerc, M. Toward a Rational Design of Poly(2,7-Carbazole) Derivatives for Solar Cells. *J. Am. Chem. Soc.* **2008**, *130*, 732−742.
(29) Kim, B.; Miyamoto, Y.; Ma, B.; Frechet, J. M. J. Photo-crosslinkable Polythiophenes for Efficient, Thermally Stable, Organic Photovoltaics. *Adv. Funct. Mater.* **2009**, *19*, 2273−2281.
(30) Chen, H.-Y.; Hou, J.; Zhang, S.; Liang, Y.; Yang, G.; Yu, L.; Wu, Y.; Li, G. Polymer Solar Cells with Enhanced Open-circuit Voltage and Efficiency. *Nat. Photonics* **2009**, *3*, 649−653.
(31) Liang, Y.; Xu, Z.; Xia, J.; Tsai, S.-T.; Wu, Y.; Li, G.; Ray, C.; Yu, L. For the Bright Future—Bulk Heterojunction Polymer Solar Cells with Power Conversion Efficiency of 7.4%. *Adv. Mater.* **2010**, *22*, E135−E138.
(32) Seo, J. H.; Gutacker, A.; Sun, Y.; Wu, H.; Huang, F.; Cao, Y.; Scherf, U.; Heeger, A. j.; Bazan, G. C. Improved High-Efficiency Organic Solar Cells via Incorporation of a Conjugated Polyelectrolyte Interlayer. *J. Am. Chem. Soc.* **2011**, *133*, 8416−8419.
(33) Wu, C.; Chiu, D. T. Highly Fluorescent Semiconducting Polymer Dots for Biology and Medicine. *Angew. Chem., Int. Ed.* **2013**, *52*, 3086−3109.
(34) Stapleton, A.; Vaughan, B.; Xue, B.; Sesa, E.; Burke, K.; Zhou, X.; Bryant, G.; Werzer, O.; Nelson, A.; Kilcoyne, A. L. D.; Thomsen, L.; Wanless, E.; Belcher, W.; Dastoor, P. A Multilayered Approach to Polyfluorene Water-based Organic Photovoltaics. *Sol. Energy Mater. Sol. Cells* **2012**, *102*, 114−124.
(35) Darwis, D.; Holmes, N.; Elkington, D.; Kilcoyne, A. L. D.; Bryant, G.; Zhou, X.; Dastoor, P.; Belcher, W. Surfactant-Free Nanoparticulate Organic Photovoltaics. *Sol. Energy Mater. Sol. Cells* **2014**, *121*, 99−107.
(36) Vandewal, K.; Gadisa, A.; Oosterbaan, W. D.; Bertho, S.; Banishoeib, F.; Severen, I. V.; Lutsen, L.; Cleij, T. J.; Vanderzande, D.; Manca, J. V. The Relation Between Open-Circuit Voltage and the Onset of Photocurrent Generation by Charge-Transfer Absorption in Polymer: Fullerene Bulk Heterojunction Solar Cells. *Adv. Funct. Mater.* **2008**, *18*, 2064−2070.
(37) Jo, J.; Kim, S.; Na, S.; Yu, B.; Kim, D. Time-Dependent Morphology Evolution by Annealing Processes on Polymer:Fullerene Blend Solar Cells. *Adv. Funct. Mater.* **2009**, *19*, 866−874.
(38) Wu, C.; Jin, Y.; Schneider, T.; Burnham, D.; Smith, P.; Chiu, D. Ultrabright and Bioorthogonal Labeling of Cellular Targets Using Semiconducting Polymer Dots and Click Chemistry. *Angew. Chem., Int. Ed.* **2010**, *49*, 9436−9440.

DOI: 10.1021/am508985q
ACS Appl. Mater. Interfaces 2015, 7, 7146−7152